

Supporting Information

Supporting Information for “Pattern self-referenced single-pixel computational holographic imaging ”

Wenjing Zhao^{a, #}, Zefang Gao^{a, #}, Zhiheng Du^a, Aiping Zhai^a, Dong Wang^{a, b, *}

a. College of Physics and Optoelectronics, Taiyuan University of Technology, No. 79 West Main Street, Yingze, 030024, China

b. Key Laboratory of Advanced Transducers and Intelligent Control System, Ministry of Education, and Shanxi Province, Taiyuan University of Technology, No. 79 West Main Street, Yingze, 030024, China

* To whom correspondence should be addressed:

wangdong@tyut.edu.cn

Supplementary Section 1: Mathematical derivation of off-axis-based PSSCH

The modulation basis employed to spatially sample the target wavefront can be a random basis or orthogonal bases like Hadamard basis, Fourier basis, discrete cosine transform (DCT) basis, and so on.

The sampling patterns $P_n(\vec{r})$ ($n \in [1, N]$) have a spatial resolution $\sqrt{N} \times \sqrt{N}$. An oblique phase grating $G(\vec{r}) = \exp(i\theta(\vec{r}))$ is designed to introduce the necessary phase difference for the off-axis interference, where i is the imaginary unit, and $\theta(\vec{r})$ is the oblique phase. Then, the encoded self-referenced patterns $E_n(\vec{r}) = P_n(\vec{r}) + G(\vec{r})$ are obtained by superposing sampling patterns with oblique phase grating. Here, each encoded self-referenced pattern is not only utilized as the spatial sampling pattern but also used to introduce the phase difference for off-axis interference. After the target wavefront $O(\vec{r}) = U(\vec{r})\exp(iV(\vec{r}))$ is modulated by an encoded pattern, the off-axis interference intensity is collected by a lens and detected by a single-pixel detector, which can be expressed as

$$\begin{aligned} y_n &= \left| \text{FFT} \{ E_n(\vec{r}) \cdot O(\vec{r}) \}_{\vec{w}=0} \right|^2 \\ &= \left| \text{FFT} \{ (P_n(\vec{r}) + G(\vec{r})) \cdot O(\vec{r}) \}_{\vec{w}=0} \right|^2 \\ &= \left| \text{FFT} \{ (P_n(\vec{r}) + e^{i\theta(\vec{r})}) \cdot O(\vec{r}) \}_{\vec{w}=0} \right|^2 \quad (\text{S1}) \\ &= \left| \iint P_n(\vec{r}) \cdot O(\vec{r}) d^2\vec{r} + \iint O(\vec{r}) \cdot e^{i\theta(\vec{r})} d^2\vec{r} \right|^2 \\ &= |S_n + C_1|^2 \end{aligned}$$

where $\text{FFT}\{\}$ represents a two-dimensional Fourier transform. \vec{r} represents the spatial coordinate vector, \vec{w} is the transform domain coordinate vector, and $\vec{w}=0$ denotes taking the zero frequency component. $S_n = \iint P_n(\vec{r}) \cdot O(\vec{r}) d^2\vec{r}$ and $C_1 = \iint O(\vec{r}) \cdot e^{i\theta(\vec{r})} d^2\vec{r}$. Although the oblique phase is related to the spatial coordinate vector \vec{r} , it is known and fixed, making C_1 can be considered to be a complex constant. Thus, y_n can also be expressed as

$$\begin{aligned}
y_n &= |S_n + C_1|^2 \\
&= |S_n|^2 + |C_1|^2 + S_n \cdot (C_1)^* + S_n^* \cdot (C_1) \\
&= I_{S_n} + I_C + I_{AC_n}
\end{aligned} \tag{S2}$$

where,

$$\begin{aligned}
I_{S_n} &= |S_n|^2 = \left| \iint P_n(\vec{r}) \cdot O(\vec{r}) d^2\vec{r} \right|^2 \\
I_C &= |C_1|^2 = \left| \iint O(\vec{r}) e^{i\theta(\vec{r})} d^2\vec{r} \right|^2 \\
I_{AC_n} &= C_1^* \iint P_n(\vec{r}) \cdot O e^{i\theta(\vec{r})} d^2\vec{r} + C_1 \iint P_n(\vec{r}) \cdot O e^{-i\theta(\vec{r})} d^2\vec{r}
\end{aligned} \tag{S3}$$

I_{S_n} and I_C represent autocorrelation, I_{AC_n} is the complex conjugate cross-correlation term. The final off-axis hologram can be reconstructed via the second-order correlation (SOC) algorithm, which can be expressed as

$$\begin{aligned}
\hat{H}(\vec{r}) &= \frac{1}{N} \sum_{n=1}^N P_n(\vec{r}) \cdot y_n \\
&= \frac{1}{N} \sum_{n=1}^N P_n(\vec{r}) \cdot (I_{S_n} + I_C + I_{AC_n}) \\
&= \frac{1}{N} \sum_{n=1}^N P_n(\vec{r}) \cdot (|S_n|^2 + |C_1|^2) + \frac{1}{N} \sum_{n=1}^N P_n(\vec{r}) \cdot [S_n \cdot C_1^* + S_n^* \cdot C_1] \\
&= \frac{1}{N} \sum_{n=1}^N P_n(\vec{r}) \cdot (|S_n|^2 + |C_1|^2) + C_1^* \cdot \frac{1}{N} \sum_{n=1}^N P_n(\vec{r}) \cdot S_n + C_1 \cdot \frac{1}{N} \sum_{n=1}^N P_n(\vec{r}) \cdot S_n^* \\
&= \frac{1}{N} \sum_{n=1}^N P_n(\vec{r}) \cdot (|S_n|^2 + |C_1|^2) + C_1^* \cdot \frac{1}{N} \sum_{n=1}^N P_n(\vec{r}) \cdot \iint P_n(\vec{r}) \cdot O(\vec{r}) d^2\vec{r} + C_1 \cdot \frac{1}{N} \sum_{n=1}^N P_n(\vec{r}) \cdot (\iint P_n(\vec{r}) \cdot O(\vec{r}) d^2\vec{r})^* \\
&= \frac{1}{N} \sum_{n=1}^N P_n(\vec{r}) \cdot (|S_n|^2 + |C_1|^2) + C_1^* \cdot \hat{O}(\vec{r}) + C_1 \cdot [\hat{O}(\vec{r})]^*
\end{aligned} \tag{S4}$$

Then, according to the Fourier fringe analysis (FFA), the spectrum of the off-axis interferogram can be obtained following the Fourier transform, subsequently, only the first-order component in the Fourier spectrum is extracted and translated to the center of the Fourier spectrum. Finally, the target wavefront can be reconstructed by conducting the inverse Fourier transform using the extracted Fourier spectrum.

Supplementary Section 2: Mathematical derivation of phase-shifting-based PSSCH

The sampling patterns $P_n(\vec{r})$ ($n \in [1, N]$) have a spatial resolution $\sqrt{N} \times \sqrt{N}$. To achieve the required phase-shifting interference, four steps of phase-shiftings, denoted as $R_\alpha = e^{i\alpha}$ ($\alpha = 0, \pi/2, \pi$ and $3\pi/2$), are encoded into the sampling patterns and thus the self-referenced patterns ($E_{n,\alpha}(\vec{r}) = P_n(\vec{r}) + R_\alpha$) can be obtained. As such, each encoded pattern can be not only utilized to spatially sample the target wavefront but also used to introduce the necessary four-step phase-shiftings. Then, the wavefront of the target object $O(\vec{r}) = U(\vec{r}) \exp(iV(\vec{r}))$ is modulated by the encoded patterns, and the phase-shifting interference intensity detected by the single-pixel detector can be expressed as

$$\begin{aligned}
I_{n,\alpha} &= \left| \text{FFT} \left\{ E_{n,\alpha}(\vec{r}) \cdot O(\vec{r}) \right\}_{\vec{w}=0} \right|^2 \\
&= \left| \text{FFT} \left\{ (P_n(\vec{r}) + R_\alpha) \cdot O(\vec{r}) \right\}_{\vec{w}=0} \right|^2 \\
&= \left| \text{FFT} \left\{ (P_n(\vec{r}) + e^{i\alpha}) \cdot O(\vec{r}) \right\}_{\vec{w}=0} \right|^2 \\
&= \left| \iint P_n(\vec{r}) \cdot O(\vec{r}) d^2\vec{r} + e^{i\alpha} \iint O(\vec{r}) d^2\vec{r} \right|^2 \\
&= |S_n + e^{i\alpha} C_2|^2
\end{aligned} \tag{S5}$$

where $S_n = \iint P_n(\vec{r}) \cdot O(\vec{r}) d^2\vec{r}$ and $C_2 = \iint O(\vec{r}) d^2\vec{r} = C_3 e^{i\beta}$, thus

$$\begin{aligned}
I_{n,\alpha} &= |S_n + C_2 e^{i\alpha}|^2 \\
&= |S_n|^2 + |C_2|^2 + S_n \cdot (C_2 e^{i\alpha})^* + S_n^* \cdot (C_2 e^{i\alpha}) \\
&= |S_n|^2 + |C_2|^2 + S_n \cdot C_2^* e^{-i\alpha} + S_n^* \cdot C_2 e^{i\alpha} \\
&= |S_n|^2 + |C_2|^2 + C_3 \left(e^{-i(\alpha+\beta)} \iint P_n(\vec{r}) \cdot O(\vec{r}) d^2\vec{r} + e^{i(\alpha+\beta)} \left[\iint P_n(\vec{r}) \cdot O(\vec{r}) d^2\vec{r} \right]^* \right) \\
&= |S_n|^2 + |C_2|^2 + C_3 \cdot \left(\iint P_n(\vec{r}) \cdot U(\vec{r}) \cdot e^{i[V(\vec{r})-\alpha-\beta]} d^2\vec{r} + \iint P_n(\vec{r}) \cdot U(\vec{r}) \cdot e^{-i[V(\vec{r})-\alpha-\beta]} d^2\vec{r} \right) \\
&= |S_n|^2 + |C_2|^2 + 2C_3 \cdot \left(\iint P_n(\vec{r}) \cdot U(\vec{r}) \cdot \cos([V(\vec{r}) - \alpha - \beta]) d^2\vec{r} \right)
\end{aligned} \tag{S6}$$

The detected intensity values corresponding to the four-step phase-shiftings can be,

$$\begin{aligned}
I_{n,0} &= |S_n|^2 + |C_2|^2 + 2C_3 \cdot \left(\iint P_n(\vec{r}) \cdot U(\vec{r}) \cdot \cos[V(\vec{r}) - \beta] d^2\vec{r} \right) \\
I_{n,\frac{\pi}{2}} &= |S_n|^2 + |C_2|^2 + 2C_3 \cdot \left(\iint P_n(\vec{r}) \cdot U(\vec{r}) \cdot \cos \left[V(\vec{r}) - \beta - \frac{\pi}{2} \right] d^2\vec{r} \right) \\
I_{n,\pi} &= |S_n|^2 + |C_2|^2 + 2C_3 \cdot \left(\iint P_n(\vec{r}) \cdot U(\vec{r}) \cdot \cos[V(\vec{r}) - \beta - \pi] d^2\vec{r} \right) \\
I_{n,\frac{3\pi}{2}} &= |S_n|^2 + |C_2|^2 + 2C_3 \cdot \left(\iint P_n(\vec{r}) \cdot U(\vec{r}) \cdot \cos \left[V(\vec{r}) - \beta - \frac{3\pi}{2} \right] d^2\vec{r} \right)
\end{aligned} \tag{S7}$$

The corresponding spectral coefficient obtained can be,

$$\begin{aligned}
y_n &= \frac{1}{4} \left[(I_{n,0} - I_{n,\pi}) + i \left(I_{n,\frac{\pi}{2}} - I_{n,\frac{3\pi}{2}} \right) \right] \\
&= C_3 \cdot \iint P_n(\vec{r}) \cdot U(\vec{r}) \cdot \cos[V(\vec{r}) - \beta] d^2\vec{r} + i \cdot C_3 \cdot \iint P_n(\vec{r}) \cdot U(\vec{r}) \cdot \sin[V(\vec{r}) - \beta] d^2\vec{r} \\
&= C_3 \cdot \iint P_n(\vec{r}) \cdot U(\vec{r}) \cdot (\cos[V(\vec{r}) - \beta] + i \cdot \sin[V(\vec{r}) - \beta]) d^2\vec{r} \\
&= C_3 \cdot \iint P_n(\vec{r}) \cdot U(\vec{r}) e^{i[V(\vec{r})-\beta]} d^2\vec{r} \\
&= C_2^* \cdot \iint P_n(\vec{r}) \cdot O(\vec{r}) d^2\vec{r}
\end{aligned} \tag{S8}$$

The target wavefront can be reconstructed using the SOC algorithm,

$$\hat{O}(\vec{r}) = \frac{1}{N} \sum_{n=1}^N P_n(\vec{r}) \cdot y_n \tag{S9}$$

Supplementary Section 3: Simulations of PSSCH using different modulation bases

The feasibility and versatility of the proposed method based on Hadamard basis, Fourier basis, and discrete cosine transform (DCT) basis are verified by simulations. The amplitude and phase of the target wavefronts, with a resolution of 128×128 pixels, are shown in Fig. S1(a) and S2(a), where the amplitudes are restricted in a circle, and the phases are represented by two images with varying phase depths, i.e. a simple binary 'leaf' and a grayscale 'house'. The simulation results employing off-axis-based PSSCH and phase-shifting-based PSSCH are shown in Fig. S1 and Fig. S2, respectively.

The simulation results demonstrate that the proposed PSSCH can reconstruct the wavefront for both simple binary and more complex grayscale targets, when using the three different modulation bases, regardless of whether it is based on the off-axis-based PSSCH or four steps phase-shifting-based PSSCH. Furthermore, it's worth noting that the method described here is not confined to the three modulation bases mentioned, it may find applicability with other modulation bases not explicitly discussed.

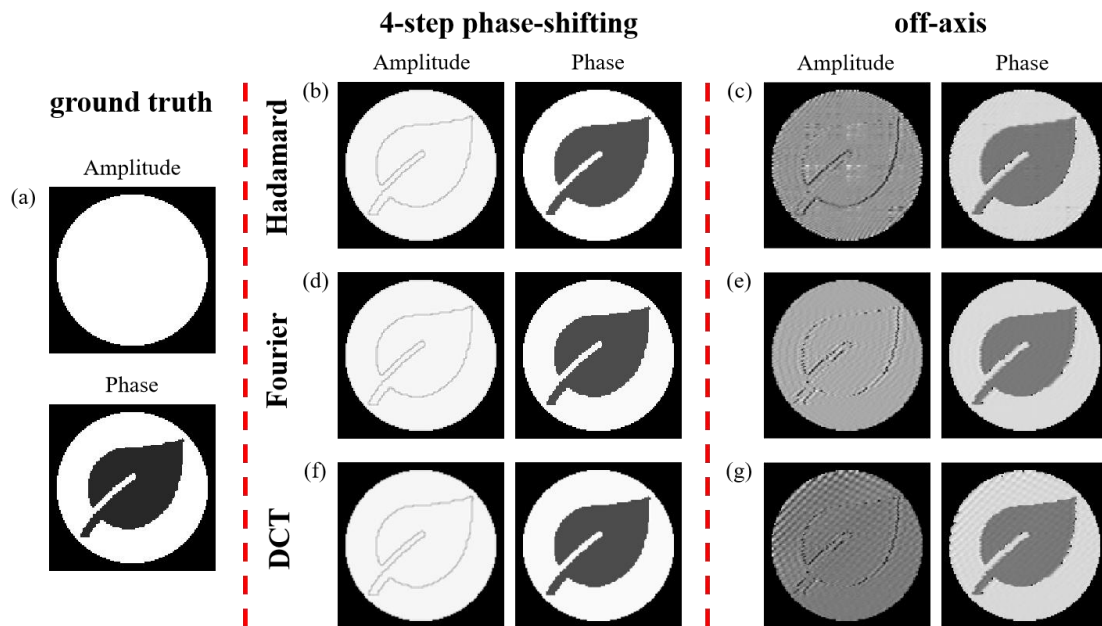


Fig. S1. The simulation results of a simple binary 'leaf' based on the Hadamard basis, Fourier basis, and DCT basis when using off-axis-based PSSCH and phase-shifting-based PSSCH. (a) Amplitude and phase of the target wavefront. Simulation results of our method using (b) - (c) the Hadamard basis, (d) - (e) the Fourier basis, and (f) - (g) the DCT basis.

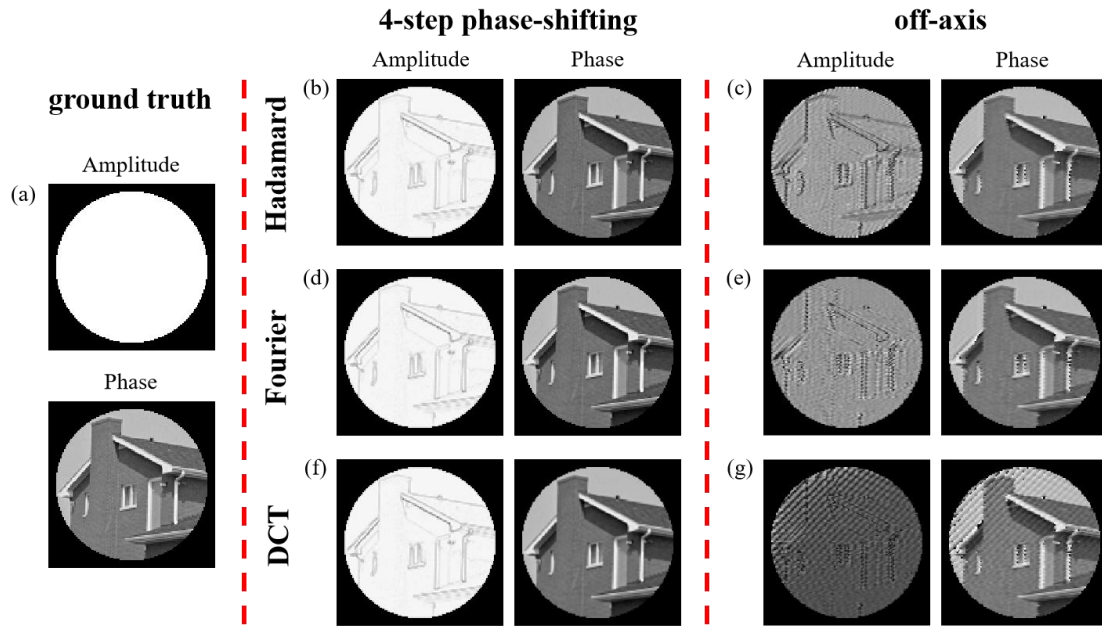


Fig. S2. The simulation results of a grayscale ‘house’ based on Hadamard basis, Fourier basis, and DCT basis when using off-axis-based PSSCH and phase-shifting-based PSSCH. (a) Amplitude and phase of the target wavefront. Simulation results of our method using (b) - (c) the Hadamard basis, (d) - (e) the Fourier basis, and (f) - (g) the DCT basis.

Supplementary Section 4: Experimental setup

The experimental setup for wavefront reconstruction is illustrated in Fig. S3. A collimated laser with a wavelength of 532 nm, expanded by a beam expander (BE), illuminates object O. The 4f optical system, consisting of lenses L₁ and L₂ with a focal length of 50 mm, relays the object's wavefront to a DMD (Vialux V-6501), which displays the sampling patterns. The wavefront modulated by the DMD is collected by the converging lens L₃ with a focal length of 150 mm, and directed to a photodetector (PD) with a 20 μm pinhole, which captures the center of the first-order diffracted light. The output is sampled by a data acquisition system (DAQ, NI DAQ USB-6216) and transmitted to a computer for image reconstruction.

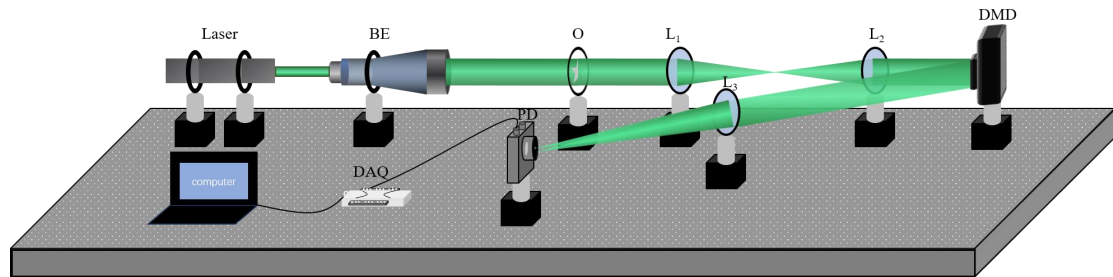


Fig. S3. Schematic of the experimental setup. Laser source of wavelength 532 nm. BE: beam expander. O: target wavefront. L₁-L₃: lens with focal lengths $f_1=50$ mm, $f_2=50$ mm, $f_3=150$ mm. DMD: digital micro-mirror device. PD: photodetector.

In the experiment, the total number of DMD pixels used is 512×512. To improve the imaging signal-to-noise ratio, 4×4 DMD pixels are merged as an imaging pixel, as a result, the final imaging solution is 128×128 pixels. The size of each DMD pixel is 7.6×7.6 μm². Thus, the size of each imaging pixel is 30.4×30.4 μm², and the imaging field of view (FOV) is 3.89×3.89 mm².